ChemComm

COMMUNICATION

View Article Online
View Journal | View Issue

Cite this: *Chem. Commun.*, 2018, **54**, 152

Received 24th October 2017,
Accepted 23rd November 2017

DOI: 10.1039/c7cc08217g

rsc.li/chemcomm

Two-color vibrational imaging of glucose metabolism using stimulated Raman scattering†

Rong Long, Luyuan Zhang, Lingyan Shi, Yihui Shen, Fanghao Hu, Chen Zeng and Wei Min *

A two-color vibrational imaging technique for simultaneously mapping glucose uptake and incorporation activity inside single living cells is reported. Heterogeneous patterns of glucose metabolism are directly visualized from the ratiometric two-color images for various cell types, cells undergoing epithelia-to-mesenchymal transitions and live mouse brain tissues. The two-color imaging of glucose metabolism here demonstrates the development of multi-functional vibrational probes for multicolor imaging of cellular metabolism.

Glucose plays a variety of important roles in both anabolic and catabolic metabolisms of cells, such as providing building blocks for cellular mass synthesis, generating ATP, and regulating intracellular redox potential. Glucose metabolism is also closely linked to metabolic transformation under various pathologic conditions. For instance, the reprogrammed glucose metabolism with enhanced aerobic glycolysis has been considered to be one of the hallmarks of cancer.[1,2]

Given the importance of glucose metabolism, multiple techniques have been developed. Positron emission tomography (PET) with radioactive glucose analogues is commonly applied in clinical diagnostics by measuring glucose uptake activity in tumors, especially with ^{18}F-deoxyglucose (FDG).[3] Magnetic resonance spectroscopy (MRS) can follow glucose metabolism *in vivo* through hyperpolarized glucose.[4,5] But both PET and MRS have limited spatial resolution for studying glucose metabolism at the cellular level. Mass spectrometry imaging (MSI) can visualize cellular glucose metabolism *via* glucose tracers,[6,7] but is a destructive approach not applicable in living systems. Fluorescence microscopy has also been applied to image glucose uptake activity with cellular resolution, using fluorescent glucose analogues.[8] However, all these techniques rely on a single probe to measure either glucose uptake or incorporation activity. Thus, they only provide partial information of glucose metabolism in cells.

Department of Chemistry, Columbia University, 3000 Broadway, New York, NY 10027, USA. E-mail: wm2256@columbia.edu

† Electronic supplementary information (ESI) available. See DOI: 10.1039/c7cc08217g

To reveal more comprehensive information of glucose metabolism, herein we report a two-color vibrational imaging approach based on both alkyne and deuterium labeled glucose analogues to simultaneously visualize glucose uptake and incorporation activity in the same living cell. We show that two-color ratiometric imaging of both glucose incorporation and uptake offers direct information on glucose utilization (*i.e.*, the efficiency of glucose incorporation into biomass) between various cell types, before and after epithelia-to-mesenchymal transition (EMT), and different regions of live brain tissue.

Stimulated Raman scattering (SRS) microscopy, as an emerging nonlinear optical imaging technique, is highly sensitive and specific in detecting chemical bonds,[9,10] with expanding application in biology.[11–13] In particular, Raman-active vibrational probes coupled with SRS microscopy provide a powerful platform for bioorthogonal chemical imaging of many small biomolecules in living systems.[14,15] Recently, two glucose analogues, 3-*O*-propargyl-D-glucose (3-OPG)[16] and D7-glucose,[17] have been separately developed to study glucose uptake activity and incorporation in lipogenesis with SRS, respectively. However, the direct combination of these two probes is difficult due to the significant spectral overlap of Raman peaks between 3-OPG (2129 cm^{-1}) and D7-glucose (broad peak between 2060 cm^{-1} and 2250 cm^{-1}).

Enlightened by the isotope-editing strategies in vibrational spectroscopy,[18–20] we expect that ^{13}C isotopic editing of the alkyne tag in 3-OPG can generate a spectrally new probe with little crosstalk with D7-glucose. Thus, we rationally designed and synthesized ^{13}C-labeled 3-*O*-propargyl-D-glucose (3-OPG-$^{13}C_3$, **1**, Fig. 1a). In order to successfully install the ^{13}C-labeled alkyne moiety *via* nucleophilic substitution, we used propargyl tosylate-$^{13}C_3$, which is prepared from commercial available propargyl alcohol-$^{13}C_3$. Deprotection under acidic conditions provided the desired 3-OPG-$^{13}C_3$ **1** in an overall 33% yield.

We first measured the spontaneous Raman spectra of the newly synthesized 3-OPG-$^{13}C_3$ in PBS (Fig. 1b, black), which shows a sharp peak at 2053 cm^{-1} in the cell Raman-silent window, indicating the Raman mode of the $^{13}C{\equiv}{}^{13}C$ stretching.

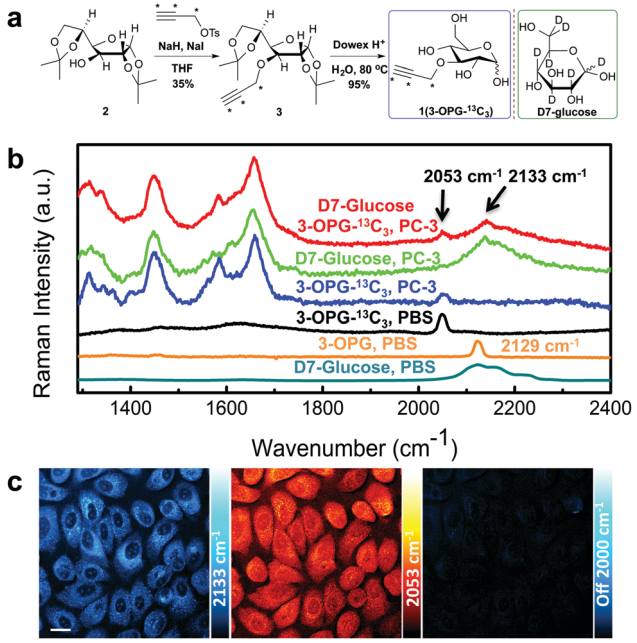

Fig. 1 Raman probes for studying the glucose metabolism. (a) Synthetic route of 3-OPG-$^{13}C_3$ and structure of D7-glucose. Stars indicate ^{13}C labeling. (b) Spontaneous Raman spectra of 1.3 M D7-glucose in PBS (dark cyan), PC-3 cells cultured with 25 mM D7-glucose for 48 hours (green), 50 mM 3-OPG in PBS (orange), 50 mM 3-OPG-$^{13}C_3$ in PBS (black), PC-3 cells cultured with 25 mM 3-OPG-$^{13}C_3$ for 2 hours (blue), PC-3 cells cultured with 25 mM D7-glucose for 48 hours and then with 25 mM 3-OPG-$^{13}C_3$ for 2 hours (red). (c) Two-color SRS imaging of PC-3 cells cultured with 25 mM D7-glucose for 48 hours and then with 25 mM 3-OPG-$^{13}C_3$ for 2 hours, indicating glucose incorporation (2133 cm^{-1}, cyan hot), glucose uptake (2053 cm^{-1}, red hot) and off-resonance (2000 cm^{-1}). Scale bar: 20 μm.

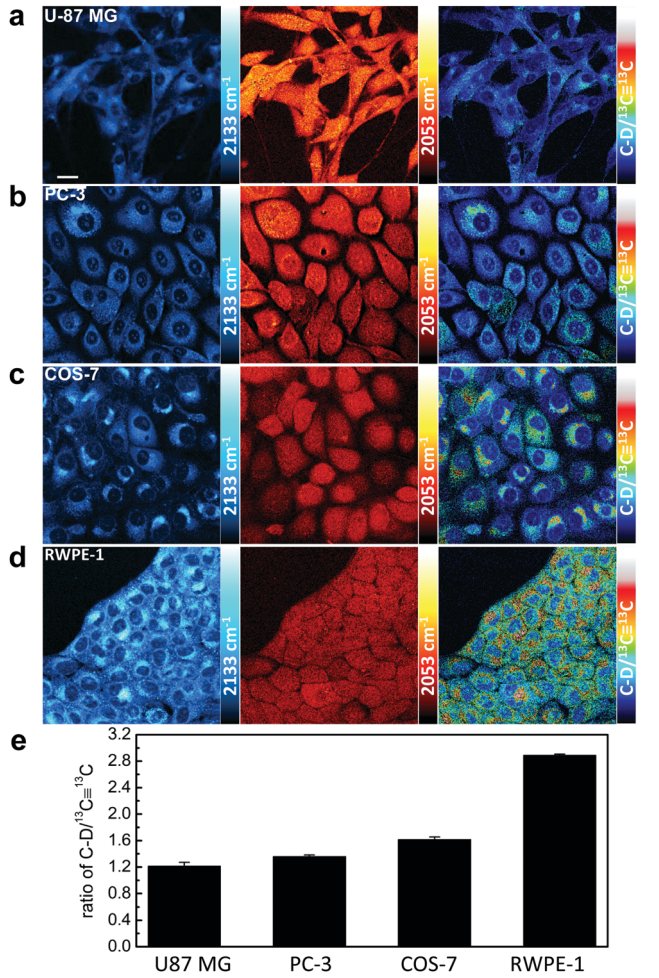

Fig. 2 Two-color glucose metabolism imaging of different cell lines. (a) U87 MG cells. (b) PC-3 cells. (c) COS-7 cells. (d) RWPE-1 cells. SRS images of glucose incorporation (C–D, cyan hot) and glucose uptake ($^{13}C\equiv{}^{13}C$, red hot), and ratiometric images (C–D/$^{13}C\equiv{}^{13}C$, royal). (e) Quantitative analysis of the ratio of C–D/$^{13}C\equiv{}^{13}C$ for different cell types. Data are shown as mean + standard deviation (SD; $n \geq 3$ replicates for each group). Scale bar: 20 μm.

The ^{13}C isotopic strategy dramatically shifted the vibrational frequency by 76 cm^{-1}, from 2129 cm^{-1} to 2053 cm^{-1}.[19,20] The spontaneous Raman spectrum and SRS images of non-treated PC-3 cells confirmed the negligible cellular background in the silent region (Fig. S1, ESI†). We also measured the uptake of 3-OPG-$^{13}C_3$ in PC-3 cells by culturing with 25 mM 3-OPG-$^{13}C_3$ for 2 hours. Indeed, an isotopic alkyne peak (2053 cm^{-1}) shows up in live cells (Fig. 1b, blue). We then tested two-color labeling in PC-3 cells with 25 mM D7-glucose for 48 hours and 25 mM 3-OPG-$^{13}C_3$ for 2 hours. These cells show two distinct peaks at 2053 cm^{-1} and 2133 cm^{-1} (Fig. 1b, red), indicating active glucose uptake and incorporation metabolism, respectively. The two Raman peaks are well resolved with $<10\%$ cross-talk (Fig. S2, ESI†). By targeting at both peaks, we can successfully visualize both glucose uptake and incorporation activity inside the same living cell *via* SRS imaging at 2053 cm^{-1} (Fig. 1c, middle panel) and 2133 cm^{-1} (Fig. 1c, left panel). The SRS image at the off-resonance frequency (2000 cm^{-1}) shows a negligible background. Thus, the newly synthesized 3-OPG-$^{13}C_3$ enables the realization of simultaneous two-color SRS imaging of glucose metabolism in single living cells.

We then demonstrated the two-color imaging of glucose uptake and incorporation activity in multiple cell lines, including human glioblastoma cells U-87 MG, human prostate cancer cells PC-3, monkey kidney cells COS-7 and human prostate normal cells RWPE-1. For each cell type, both glucose incorporation and uptake activity are imaged in the same set of living cells (Fig. 2a–d), with 3-OPG-$^{13}C_3$ evenly distributed throughout the cells and D7-glucose incorporated into intracellular structures. We also calculated the ratiometric images (C–D/$^{13}C\equiv{}^{13}C$) for each cell to quantitatively visualize the efficiency of glucose incorporation into the biomass at the single cell level (Fig. 2a–d, right panel). Based on the quantitative analysis (Fig. 2e), the prostate normal cells RWPE-1 exhibit the highest ratio (2.89 ± 0.01). In contrast, the glioblastoma cancer cells U-87 MG show the lowest ratio (1.21 ± 0.05). Thus, normal cells have higher anabolic activity for biomass synthesis, and cancer cells have more catabolic activity for fast energy production when using glucose. The ratiometric images based on the two-color SRS technique can directly reveal the inherent difference of glucose utilization and the metabolic pathway between normal and cancer cells.

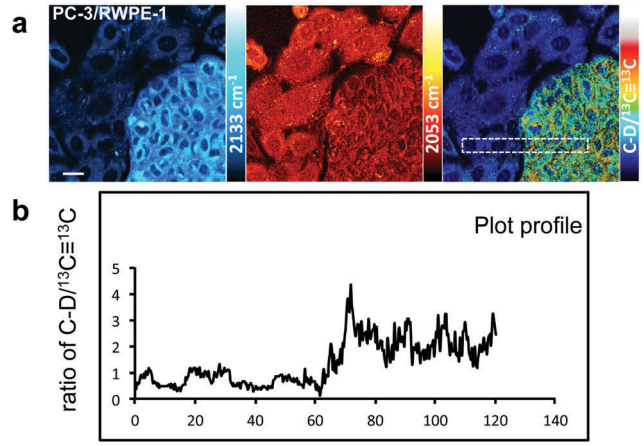

Fig. 3 Two-color imaging of glucose metabolism in co-cultured prostate cells. (a) SRS images of the co-culture PC-3/RWPE-1. SRS images of glucose incorporation (C–D, cyan hot) and glucose uptake ($^{13}C\equiv{}^{13}C$, red hot), and ratiometric image (C–D/$^{13}C\equiv{}^{13}C$, royal). (b) Plot profile of the dashed region (average in the vertical direction) in the ratiometric image. Scale bar: 20 μm.

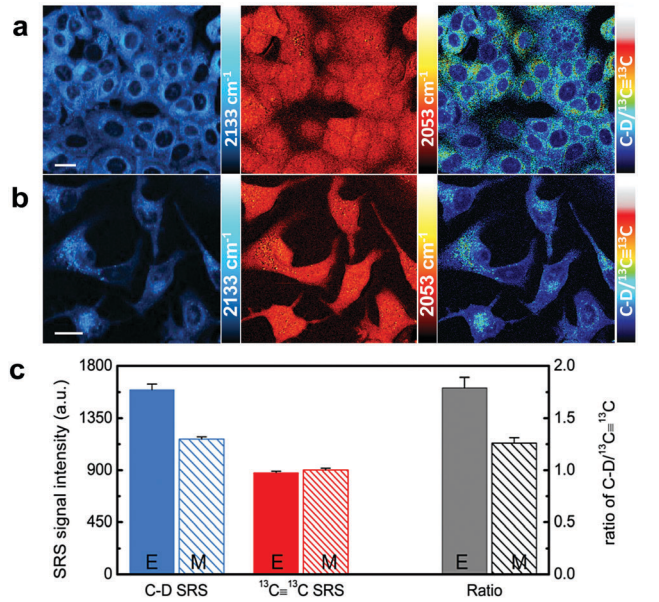

Fig. 4 Two-color glucose metabolism imaging of MCF-7 cells with epithelia-to-mesenchymal transition (EMT). (a) Epithelial MCF-7 cells. (b) Mesenchymal MCF-7 cells. (c) Quantitative analysis of the C–D signal, $^{13}C\equiv{}^{13}C$ signal and the ratio of C–D/$^{13}C\equiv{}^{13}C$ for epithelia and mesenchymal cells. Data are shown as mean + standard deviation (SD; $n \geq 3$ replicates for each group). p values of Student's t-test: $p < 0.0001$; $p > 0.2$; $p < 0.001$ (from left to right). Scale bar: 20 μm.

We further showed that the two-color imaging of glucose metabolism could be applied to the co-culture of cancer cells PC-3 and normal cells RWPE-1 of the same prostate tissue origin (Fig. 3). In the co-culture system, the profile of a specified region in the ratiometric image shows a significantly higher ratio of glucose incorporation into the biomass in RWPE-1 than in PC-3. The lower glucose incorporation activity in the cancerous PC-3 might be attributed to the Warburg effect, which has upregulated aerobic glycolysis and lactate secretion rather than anabolic biomass synthesis.[21]

D-7 glucose has been shown to be incorporated into cellular lipids.[17] We verified that *de novo* lipogenesis is indeed the major metabolic pathway of D-7 glucose[17] using an inhibitor of fatty acid synthase, TVB-3166,[22] in prostate normal cells RWPE-1 (Fig. S3, ESI†) and cancer cells PC-3 (Fig. S4, ESI†). 10 μM TVB-3166 could dramatically decrease the glucose incorporation after 24 hours of treatment without the influence on glucose uptake activity in both cell lines, resulting in significant reduction in the C–D/$^{13}C\equiv{}^{13}C$ ratio by ~63% (RWPE-1) and 27% (PC-3) (Fig. S3 and S4, ESI†).

The epithelial-to-mesenchymal transition (EMT) process, encompassing the conversion of epithelial cells to invasive mesenchymal cells, plays an important role in cancer metastasis.[23] We next applied the two-color SRS imaging of both glucose uptake and incorporation activity in detecting the altered glucose metabolism during EMT (Fig. 4). The EMT in MCF-7 cells is confirmed by immunofluorescence (Fig. S5, ESI†).[24] The SRS images show that glucose incorporation into the cellular lipids is dramatically decreased after EMT, while the glucose uptake activity is not significantly changed (Fig. 4c). Quantitative analysis of the ratiometric images reveals 30% reduction in the C–D/$^{13}C\equiv{}^{13}C$ ratio during EMT. Compared to the epithelial state, this suggests that the cells in the mesenchymal state utilize less glucose for biomass synthesis and possibly more for catabolic metabolism and energy production to support the high-energy requirement of cell mobility during EMT.[25] The demonstration here suggests that the ratiometric two-color SRS imaging of glucose metabolism might provide a sensitive tool for detecting circulating tumor cells and their metabolism during cancer metastasis at the single-cell level.

Lastly, we demonstrated the two-color SRS imaging of glucose metabolism in *ex vivo* live mouse brain tissues with both D7-glucose and 3-OPG-$^{13}C_3$ probes. The choroid plexus (CP) is responsible for the production of cerebrospinal fluids (CSF), which is of great importance for the development and maintenance of the central nervous system.[26] The distinct activity of glucose metabolism in CP is directly visualized by SRS for the first time. Label-free SRS images show the distributions of lipids (CH_2, green), proteins (CH_3, blue) and their merged pattern (Fig. 5a). CP is identified by its unique morphology and its high protein but low lipid content (white-solid line). Pronounced signals are present in both the glucose incorporation channel (C–D, cyan hot) and glucose uptake ($^{13}C\equiv{}^{13}C$, red hot) channel (Fig. 5b). The ratiometric image (Fig. 5b, right panel) exhibits elevated glucose incorporation in the CP region when compared with the nearby brain tissue (yellow-solid line). Additionally, in the magnified images, the CP epithelial cells (Fig. 5c, arrow-headed) clearly show the polarization with diminished activity on the apical side (facing the brain ventricle) and elevated activity on the basolateral side (facing central stroma). Importantly, such asymmetry is required for the sorting and trafficking of the CSF component.[27] Therefore, two-color SRS imaging of both glucose uptake and incorporation activity is applicable in live brain tissues with subcellular resolution.

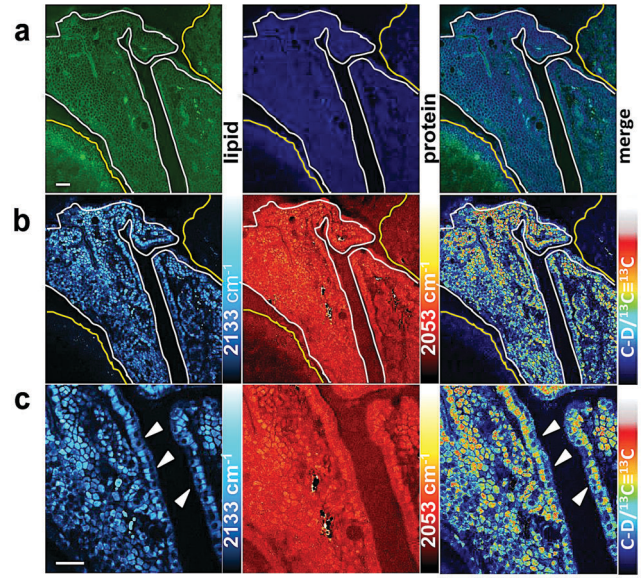

Fig. 5 Two-color glucose metabolism imaging of choroid plexus (CP) in *ex vivo* live mouse brain tissues. (a) SRS images of lipid (CH_2, green), protein (CH_3, blue) and merged one. (b) SRS images of glucose incorporation (C–D, cyan hot) and glucose uptake ($^{13}C{\equiv}{}^{13}C$, red hot), and ratiometric image (C–D/$^{13}C{\equiv}{}^{13}C$, royal). CP shown as the white-solid line region and the nearby brain tissue shown as the yellow-solid line region. (c) SRS images of 2× zoomed in of the CP region (CP epithelial cells, arrow-headed). Scale bar: 20 μm.

In summary, we have presented a two-color SRS imaging approach to study both the glucose uptake and incorporation activity in living cells and mouse brain tissues with high specificity, resolution and biocompatibility. With a ^{13}C-isotope editing strategy, the new 3-OPG-$^{13}C_3$ probe not only preserves the characteristics of the original 3-OPG probe for visualizing glucose uptake activity, but also provides a new Raman frequency to be spectrally resolved from the other glucose probe, D7-glucose for incorporation activity. The combination of these two vibrational probes thus provides a complete set to simultaneously study glucose uptake and incorporation activity with SRS microscopy. We have also shown that the two-color ratiometric images could be used as a quantitative visualization of glucose utilization and the contribution of biomass incorporation in living systems with subcellular resolution. We further anticipate that this technique can serve as a useful tool in cancer diagnostics and therapeutic development by selectively targeting the reprogrammed glucose metabolism.[2,28]

W. M. acknowledges support from an NIH Director's New Innovator Award (Grant 1DP2EB016573), NIH R01 (Grant EB020892), the US Army Research Office (W911NF-12-1-0594), the Alfred P. Sloan Foundation, and the Camille and Henry Dreyfus Foundation.

Conflicts of interest

There are no conflicts to declare.

Notes and references

1 P. S. Ward and C. B. Thompson, *Cancer Cell*, 2012, **21**, 297–308.
2 N. Hay, *Nat. Rev. Cancer*, 2016, **16**, 635–649.
3 S. Ben-Haim and P. Ell, *J. Nucl. Med.*, 2009, **50**, 88–99.
4 T. B. Rodrigues, E. M. Serrao, B. W. Kennedy, D. E. Hu, M. I. Kettunen and K. M. Brindle, *Nat. Med.*, 2014, **20**, 93–97.
5 L. Lumata, C. Yang, M. Ragavan, N. Carpenter, R. J. DeBerardinis and M. E. Merritt, *Methods Enzymol.*, 2015, **561**, 73–106.
6 J. Wang, S. Qiu, S. Chen, C. Xiong, H. Liu, J. Wang, N. Zhang, J. Hou, Q. He and Z. Nie, *Anal. Chem.*, 2015, **87**, 422–430.
7 C. T. Hensley, B. Faubert, Q. Yuan, N. Lev-Cohain, E. Jin, J. Kim, L. Jiang, B. Ko, R. Skelton, L. Loudat, M. Wodzak, C. Klimko, E. McMillan, Y. Butt, M. Ni, D. Oliver, J. Torrealba, C. R. Malloy, K. Kernstine, R. E. Lenkinski and R. J. DeBerardinis, *Cell*, 2016, **164**, 681–694.
8 K. Yamada, M. Saito, H. Matsuoka and N. Inagaki, *Nat. Protoc.*, 2007, **2**, 753–762.
9 C. W. Freudiger, W. Min, B. G. Saar, S. Lu, G. R. Holtom, C. He, J. C. Tsai, J. X. Kang and X. S. Xie, *Science*, 2008, **322**, 1857–1861.
10 J. X. Cheng and X. S. Xie, *Science*, 2015, **350**, aaa8870.
11 W. Min, C. W. Freudiger, S. Lu and X. S. Xie, *Annu. Rev. Phys. Chem.*, 2011, **62**, 507–530.
12 C. S. Liao and J. X. Cheng, *Annu. Rev. Anal. Chem.*, 2016, **9**, 69–93.
13 R. C. Prince, R. R. Frontiera and E. O. Potma, *Chem. Rev.*, 2017, **117**, 5070–5094.
14 L. Wei, F. Hu, Z. Chen, Y. Shen, L. Zhang and W. Min, *Acc. Chem. Res.*, 2016, **49**, 1494–1502.
15 Z. Zhao, Y. Shen, F. Hu and W. Min, *Analyst*, 2017, **142**, 4018–4029.
16 F. Hu, Z. Chen, L. Zhang, Y. Shen, L. Wei and W. Min, *Angew. Chem., Int. Ed.*, 2015, **54**, 9821–9825.
17 J. Li and J. X. Cheng, *Sci. Rep.*, 2014, **4**, 6807.
18 Z. Liu, X. Li, S. M. Tabakman, K. Jiang, S. Fan and H. Dai, *J. Am. Chem. Soc.*, 2008, **130**, 13540–13541.
19 Z. Chen, D. W. Paley, L. Wei, A. L. Weisman, R. A. Friesner, C. Nuckolls and W. Min, *J. Am. Chem. Soc.*, 2014, **136**, 8027–8033.
20 L. Wei, Z. Chen, L. Shi, R. Long, A. V. Anzalone, L. Zhang, F. Hu, R. Yuste, V. W. Cornish and W. Min, *Nature*, 2017, **544**, 465–470.
21 Y. J. Chen, X. Huang, N. G. Mahieu, K. Cho, J. Schaefer and G. J. Patti, *Biochemistry*, 2014, **53**, 4755–4757.
22 R. Ventura, K. Mordec, J. Waszczuk, Z. Wang, J. Lai, M. Fridlib, D. Buckley, G. Kemble and T. S. Heuer, *Biomedicine*, 2015, **2**, 808–824.
23 R. Huang and X. Zong, *Crit. Rev. Oncol. Hematol.*, 2017, **115**, 13–22.
24 L. Zhang and W. Min, *J. Biomed. Opt.*, 2017, **22**, 1–7.
25 L. Jiang, R. Deberardinis and D. A. Boothman, *Mol. Cell. Oncol.*, 2015, **2**, e981994.
26 M. P. Lun, E. S. Monuki and M. K. Lehtinen, *Nat. Rev. Neurosci.*, 2015, **16**, 445–457.
27 I. B. Christensen, T. Gyldenholm, H. H. Damkier and J. Praetorius, *Front. Physiol.*, 2013, **4**, 344.
28 S. E. Elf and J. Chen, *Cancer*, 2014, **120**, 774–780.